JOURNAL OF OPTOELECTRONICS AND ADVANCED MATERIALS, Vol. 12, No. 6, June 2010, p. 1279 - 1285

Microstructure DC resistivity and magnetic property of Ni-Zn ferrite nano-powders synthesized by EDTA precursor based method

P. P. SARANGI[a], S. R. VADERA[b], M. K. PATRA[b], N. N. GHOSH[a*]
[a]*Chemistry Group, Birla Institute of Technology and Science – Pilani, Goa Campus, Zuarinagar – 403726, India*
[b]*Defence Lab, Rajasthan, Jodhpur 342011, India*

$Ni_{1-x}Zn_xFe_2O_4$ ($0 \le x \le 1$) nanopowders (average particle size ~ 30 nm) have been synthesized by using a ethylenediamine tetraacetic acid precursor based method. The synthesized nanopowders were obtained by calcining the precursors in air at 450^0C. Microstructures of the nanopowders and samples obtained on sintering have been studied by using Scanning Electron Microscopy. DC electrical resistivity was found to be ~10^7Ωcm for the as-synthesized nanopowders and ~10^6 Ωcm for sintered samples. Room temperature magnetization has also been measured for all compositions and it exhibits a decrease with increasing Zn content in the samples.

(Received May 25, 2010; accepted June 16, 2010)

Keywords: Ferrite, Nanopowders, Microstructure, SEM, Resistivity

1. Introduction

Ferrites are magnetic materials that have long been in use for numerous technological applications [1]. In recent years, nano-structured ferrites and their composites [2] have emerged as materials of interest. They have the potential to exhibit certain superior properties that could lead to novel applications in the field of high frequencies, antennas, transformer cores etc. Magnetic nanoparticles dispersed in a liquid carrier (e.g. ferrofluids) have potential to be used in many biomedical applications such as targetted drug delivery, contrast enhancement for Magnetic Resonance Imaging (MRI), magnetic seperation of cells etc. [3].

Although there is a spectrum of applications for these nanomaterials, it is not easy to produce ferrites with good homogeneity and desirable properties. Ferrites are known to be highly structure-sensitive materials and their properties greatly depend on the synthesis routes. We have reviewed several synthetic routes for synthesis of different ultrafine ferrite powders and references are cited therein [4]. Solid State route has been the traditional method to prepare ferrite powders but it is inept of producing nanostructured ferrites. Conventional wet chemical methods such as co-precipitation, sol-gel, hydrothermal, precursor based methods etc. are capable of producing nano-structured ferrite powders. However, they are associated with some inherent limitations such as use of expensive metal alkoxides or complex metal compounds, frequent use of strong acids/bases and organic solvents, formation of heterogeneous/undesirable crystalline phases during processing etc.

In order to surmount the limitations associated with other reported methods, we have developed aqueous solution based chemical methods to synthesize single phase α-Fe_2O_3 and Ni-Zn ferrite nanopowders [5-11]. The importance of single phase material should not be undermined as the electrical and magnetic properties of ferrites are highly sensitive to the purity of phase of the synthesized material. These physical properties, to a large extent, also depend on the synthesis route, microstructures, sintered density and sintering temperature etc. The resistivity of bulk Ni-Zn ferrites and its dependence on temperature, microstructure and sintering conditions etc. has been reported by some researchers [12-17]. But a systematic study of resistivity of nanostructured Ni-Zn ferrites is still required to establish structure- property relationship.

In view of above, we have undertaken a comprehensive investigation of the variation of DC resisitivity with microstructure, sintering temperature, and composition (x = 0.20 to 0.60) of the synthesized $Ni_{1-x}Zn_xFe_2O_4$ nanopowders, prepared by the EDTA precursor based method. The resistivity behavior of the as synthesized nanopowders has been correlated with change of microstructures evolved during their sintering. Room temperature magnetization has also been measured for all compositions by using VSM (Vibrating Sample Magnetometer).

2. Experimental procedure

The chemicals used were $Fe(NO_3)_3.9H_2O$ (99.9%, Merck, India), $Ni(NO_3)_2.6H_2O$ (99.9%, Merck, India), Zn powder (99.9%, Merck, India), and ethylenediamine tetracetic acid (EDTA, 99.9%, Merck, India) without further purification. $Zn(NO_3)_2$ was prepared by dissolving

Zn powder in aqueous nitric acid. Stoichiometric amounts of metal nitrates were dissolved in distilled water according to the molar compositions as shown in Table 1.

Table 1. Molar ratio of starting compounds

Target Composition	$Fe(NO_3)_3.9H_2O$	$Ni(NO_3)_2.6H_2O$	Zn	EDTA
$Ni_{0.80}Zn_{0.20}Fe_2O_4$	0.084	0.034	0.008	0.126
$Ni_{0.65}Zn_{0.35}Fe_2O_4$	0.084	0.027	0.015	0.126
$Ni_{0.50}Zn_{0.50}Fe_2O_4$	0.084	0.021	0.021	0.126
$Ni_{0.40}Zn_{0.60}Fe_2O_4$	0.084	0.017	0.025	0.126

Aqueous solutions of metal nitrates and EDTA were mixed in a molar ratio of 1:1. The solutions were stirred for 1hour at room temperature using a magnetic stirrer. Dark brown precursors were formed when the mixtures were evaporated to dryness on a hot plate at ~125^{0}C. The precursor powders were then calcined in air in temperatures ranging from 250 to 450^{0}C for 2.30 hours to obtain Ni-Zn ferrite nanopowders [9].

Thermo gravimetric Analysis (TGA) and Differential Scanning Calorimetric (DSC) analysis were carried out for the precursors by using Shimadzu DTG–60 and Shimadzu DSC–60 respectively. X-Ray Diffraction (XRD) spectra of the precursors and the calcined powders for all compositions were recorded by using a Rigaku Powder X-Ray Diffractometer (Mini Flex II) with Cu K_α (λ = 0.15405 nm) radiation. The particle size for the calcined powder was determined by using a Field Emission Gun Transmission Electron Microscope (JEOL JEMS FEG-TEM, -2100). Morphology of the calcined powders was studied using JEOL Scanning Electron Microscopy (JSM-6360LV). DC resistivity was measured from room-temperature to 225^{0}C by the two-probe method using a Keithley Electrometer (6517 A). For this measurement, powder was pressed into pellets of ~13mm diameter and ~ 2 mm thickness by applying a pressure of 3 tons. The pellets were coated on both surfaces with silver for resistivity measurements. The green density and sintered density of the pellets were measured by using the dimensions of the pellet [18]. Room temperature magnetization with respect to external magnetic field was measured for powders calcined at 450^{0}C for all compositions by using Vibrating Sample Magnetometer (EV5, ADE Technology, USA).

3. Results and discussion

3.1 Thermal analysis

The thermal decomposition behavior of the precursors was investigated by using TG-DSC analysis and the thermograms for $Ni_{1-x}Zn_xFe_2O_4$ (x = 0.35) are shown in Fig.1 as representative.

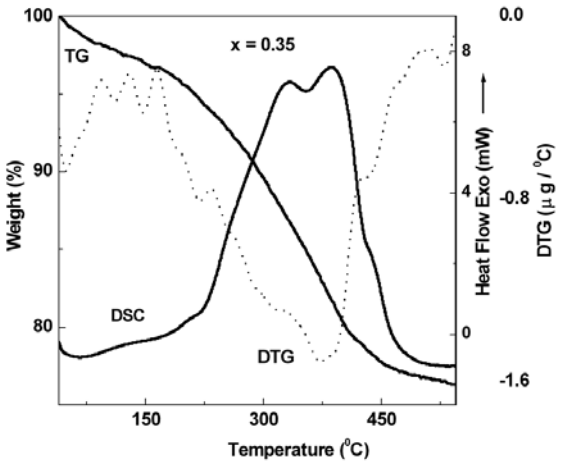

Fig. 1. TG-DTG and DSC thermograms for precursor powders of $Ni_{0.65}Zn_{0.35}Fe_2O_4$ in air

From TGA, a total weight loss of ~25% was observed when the sample was heated between 40 to 550^{0}C in air. Minor weight loss ~5% occurred between 30 and 150^{0}C that can be assigned to the loss of moisture from the samples. Major weight loss of ~20% occurred in the region from 150 to 460^{0}C and this weight loss was attributed to oxidative decomposition of precursor, accompanied by the evolution of CO_2 and NO_x gases. Heating the sample beyond 460^{0}C showed neither a significant weight loss in TGA nor formation of any new peak in DSC, confirming the completion of decomposition of the precursor to iron oxide at ~460^{0}C. The nature of TG-DTG-DSC thermograms for all compositions was similar and confirmed full decomposition of the precursors to corresponding ferrite powders at 450^{0}C. The heat liberated (1 to 3 kJ/g, depending upon the composition) through this process was sufficient for the crystallization of the desired ferrite phase [9, 21].

3.2 X-Ray Analysis:

Room temperature XRD spectra of the precursors and the powders calcined at different temperatures was recorded for the whole series of synthesized Ni-Zn ferrites. XRD spectra of $Ni_{1-x}Zn_xFe_2O_4$ precursors and calcined powders are shown in Fig. 2.

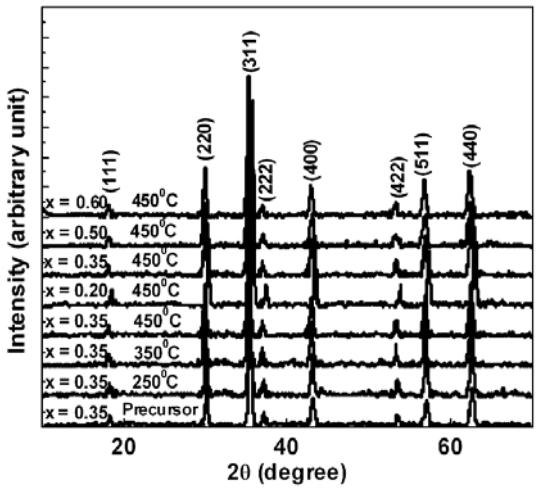

Fig. 2. X-ray diffraction spectra of precursor, calcined powders of $Ni_{0.65}Zn_{0.35}Fe_2O_4$ and powders calcined at 450^0C for the series of composition $Ni_{1-x}Zn_xFe_2O_4$

The presence of peaks corresponding to (111), (220), (311), (222), (400), (422), (511) and (440) diffraction planes confirmed the formation of single-phase Ni-Zn ferrite (JCPDS 08-0234). The striking feature was the formation of pure ferrite phase in the precursor. The crystallite sizes, calculated by using Scherrer's equation, varied between 15-30 nm depending upon compositions and calcination temperatures.

3.3 TEM Analysis

Transmission Electron Microscopy (TEM) was performed for the series of synthesized nanopowders obtained by calcination of the precursors at 450^0C. The TEM micrographs of the calcined powders (x = 0.50 and 0.60 as representatives are shown in Fig. 3) indicated that average particle size of the as-synthesized nanopowder was ~30 nm. The particles were rounded in shape and formed loose aggregates.

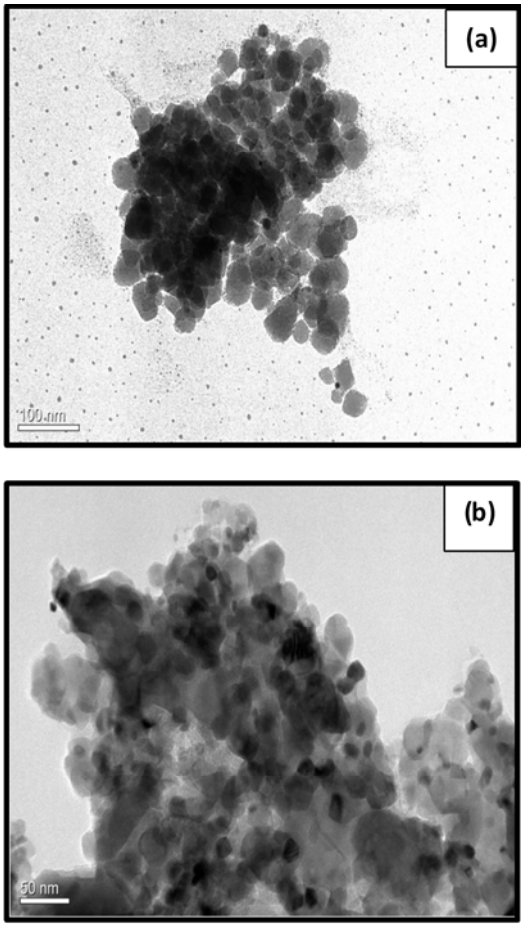

Fig. 3 TEM micrographs for the series of $Ni_{1-x}Zn_xFe_2O_4$ of nanopowders for (a) x = 0.50 and (b) x = 0.60, synthesized at calcination temperature of 450^0C

3.4 SEM Analysis

SEM was used to investigate the change of microstructures of the as synthesized $Ni_{1-x}Zn_xFe_2O_4$ nanopowders with change in sintering temperature and composition and these are shown in Fig 4 (a-i). For this purpose, four sets of pellets were prepared, (i) one pellet was kept unsintered (ii) the other set of pellets were sintered at 1100, 1200 and 1300^0C for 2 hours in air atmosphere.

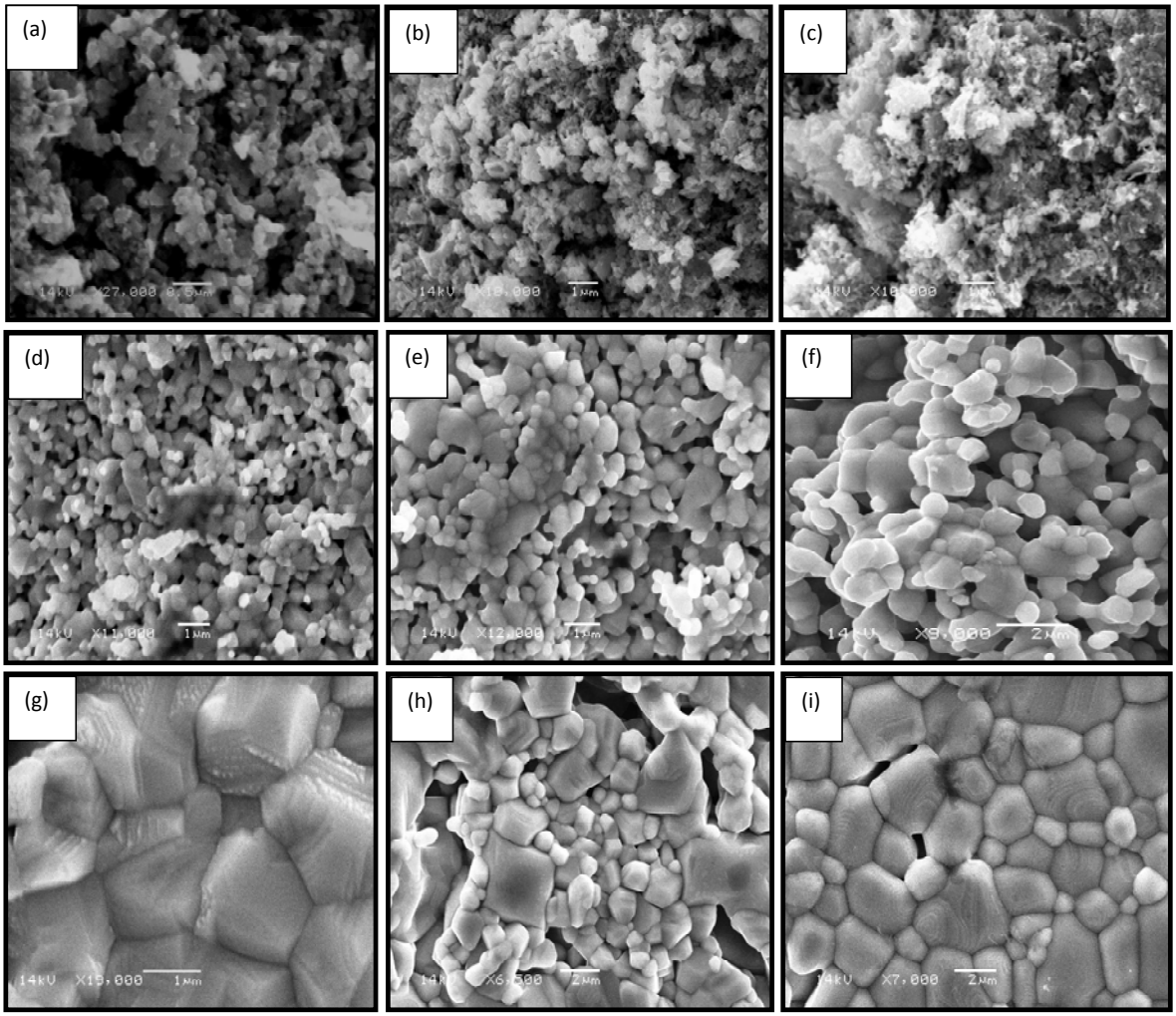

Fig.4 SEM micrographs of $Ni_{(1-x)}Zn_xFe_2O_4$ showing the change of microstructure with changing value of x and sintering condition (a) x = 0.20, unsintered, (b) x = 0.35, unsintered, (c) x = 0.60, unsintered, (d) x = 0.35, sintered at 1100^{0}C, (e) x = 0.50, sintered at 1100 ^{0}C, (f) x = 0.20, sintered at 1200 ^{0}C, (g) x = 0.60, sintered at 1200 ^{0}C, (h) x = 0.20, sintered at 1300^{0}C, (i) x = 0.60, sintered at 1300^{0}C

SEM micrographs exhibiting evolution of microstructure with change in composition and sintering temperature are shown in Fig. 4 (a-i) and discussed below:

(i) SEM micrographs of the as-synthesized samples exhibited uniform and loosely agglomerated particles of Ni-Zn ferrite powders (Fig 4 a-c). (ii) When sintering was performed at 1100^{0}C, beginning of grain growth was clearly observed in the micrographs. The nanoparticles grew to micron sized grains and they were rounded in shape. They were also found to be agglomerated and exhibited lots of intergranular porosity (Fig 4 d-e). (iii) Sintering at 1200^{0}C resulted in formation of well defined, bigger grain sizes (~2 microns) with reduction in porosity and lessened amount of agglomeration (Fig 4 f). The effect of increase in Zn concentration (x = 0.60) was well reflected in Fig 4g where densification occured to a greater extent as compared to the sample with less Zn concentration (x = 0.20, Fig 4f). Inhomogeneity or partial precipitation of any impurity phase was not observed for any of these samples. (iv) When sintering was performed at 1300^{0}C, grain size distribution became non-uniform, particularly when concentration of Zn is high (Fig 4 h-i). The microstructures for the samples sintered at 1300^{0}C were dominated by preferential grain growth. It should also be noted that, though sintering temperature was reasonably high (1300^{0}C), Zn loss was not observed in the form of pores inside the grains in our samples. Zn loss at this high temperature has been reported in SEM micrographs in the form of intragranular porosity [18]. This ensures the maintenance of stoichiometry of the as-synthesized samples at very high temperatures.

3.5 DC Resistivity measurement

DC resistivity of the unsintered and sintered pellets was measured from room temperature to 225^{0}C by using the two-probe method for all values of x (Fig. 5).

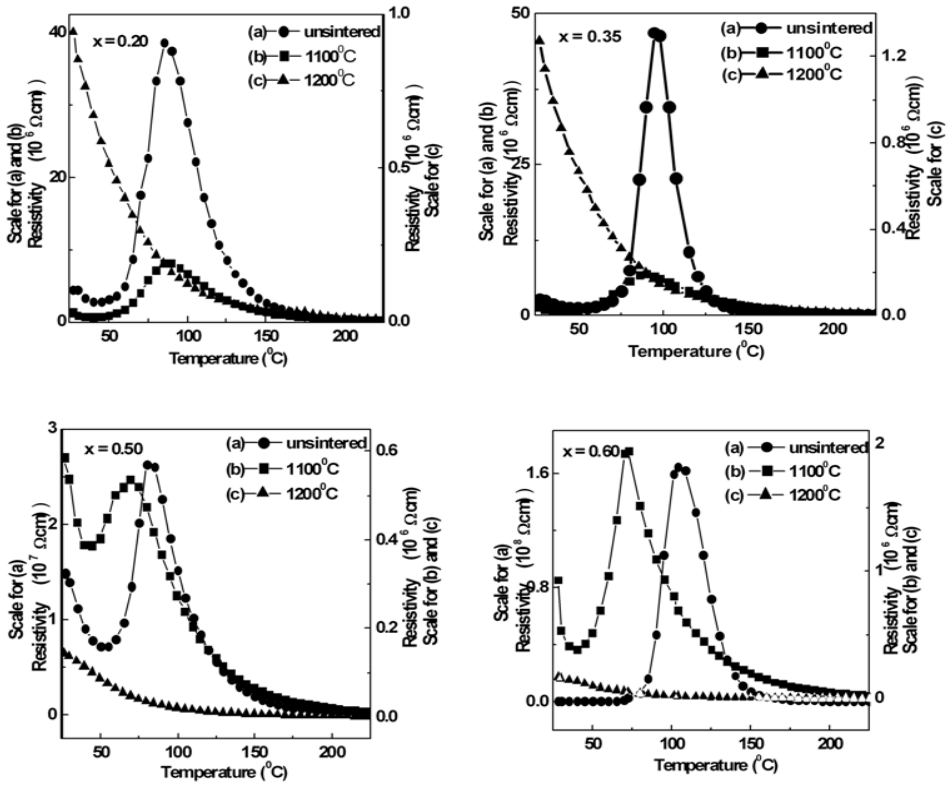

Fig.5 DC resistivity for the series of $Ni_{1-x}Zn_xFe_2O_4$ nanopowders with respect to temperature for unsintered samples and samples sintered at 1100 and 1200^{0}C

The resistivity behavior for the series of $Ni_{1-x}Zn_xFe_2O_4$ ($0 \le x \le 1$) powders with respect to temperature is described below for unsintered and sintered cases:

(i) Unsintered Sample:

It was observed that the room temperature resistivity of the unsintered samples was of the order of ~10^5-10^7Ωcm depending upon the composition of the nanopowders. With increase in temperature, the resisitivity increased and a maximum was recorded in the temperature range of ~ 80-100^{0}C. This behavior might be attributed to the presence of open porosity, loose agglomeration of ultrafine powders and entrapped moisture inside the pores of the powders [19, 21] (humidity recorded in our lab was ~91% at room temperature). Increasing the temperature upto ~100^{0}C caused the evaporation of moisture from the samples and therefore, maximum resistivity (~10^7-10^8 Ωcm) was attained. This maximum in resistivity corresponds to desorption of moisture from the samples. After ~100^{0}C, the samples exhibited typical negative temperature coefficient of resistance (NTCR) behavior of ferrites [13]. Such high resistivities can be explained by simply understanding the fact that smaller grains would offer greater resistance to electron path.

(ii) Sintering at 1100^{0}C:

When the samples were sintered at 1100^{0}C, the grains grew in size and also the porosity was reduced (Fig. 4(d-e)). Therefore, the impact of adsorption of moisture in these samples was also less pronounced. This was clearly reflected from Fig. 5 where the peak in the resistivity curve shifted to a lower temperature for all values of x in comparison to the unsintered samples. This was due to the presence of less number of pores present in the sintered samples. Hence, complete elimination of moisture occured at a comparatively lower temperature (<100^{0}C).

(ii) Sintering at 1200^{0}C:

The microstructures of samples sintered at 1200^{0}C were homogenous with large grain sizes. Absence of any intergranular or intragranular porosity especially for higher Zn concentration (x = 0.60) was observed (Fig 4(f-g)). Therefore, these samples exhibited typical NTCR behavior of ferrites from room temperature to 225^{0}C. With increasing amount of Zn, a decrease in room temperature resistivity for all samples was observed. This is because zinc is known to promote densification and grain growth in the samples and large grains with lesser number of grain boundaries would cause a decrease in the resistivity [18].

3.6 Magnetic measurement

We have measured the room temperature saturation magnetization (M_s) and coercivity (H_c) of the as-synthesized nanopowders, calcined at 450^0C, using VSM (Fig. 6).

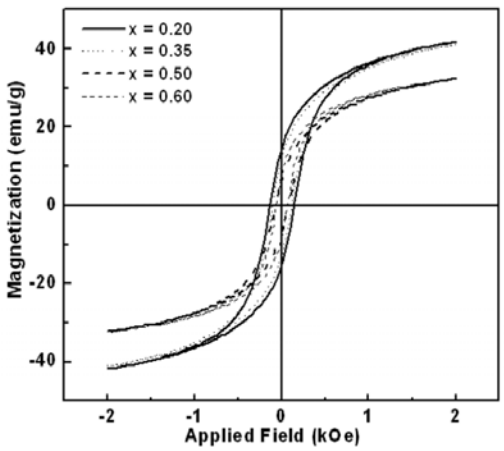

Fig.6 Room temperature hysteresis loops for the series of $Ni_{1-x}Zn_xFe_2O_4$ nanopowders

The measured values for the series of composition $Ni_{1-x}Zn_xFe_2O_4$ ($0.2 \leq x \leq 0.60$) are listed in Table 2.

Table 2.Variation of room temperature saturation magnetization and coercivity with composition for the as synthesized nanopowders.

$Ni_{1-x}Zn_xFe_2O_4$	M_s (emu/g)	H_c (Oe)
x = 0.20	41.9	132
x = 0.35	41.2	103.5
x = 0.50	32.4	64.6
x = 0.60	32.4	65

It was observed that saturation magnetization decreased with increasing Zn^{2+} concentration (x= 0.20 - 0.60) from 41.9 to 32.4 emu/g. Zn^{2+} ions have an affinity to occupy tetrahedral (A) sites and Ni^{2+} ions have a tendency to go into the octahedral (B) sites in the crystal lattice [22], while Fe^{3+} ions are distributed over both the sites. It might happen that as the concentration of diamagnetic Zn^{2+} on A sites is increased, the Fe^{3+} ions were pushed from A to B sites. This decrease in the magnetic ions at A site resulted in a weakened A-B exchange coupling and hence a diminished moment [23].

TGA-DSC, XRD and TEM analysis of the synthesized precursors and calcined powders confirmed that oxidative decomposition of precursor leads to the formation of single phase Ni-Zn ferrite nanopowders. In this chemical method, a homogeneous aqueous solution of metal nitrates and EDTA, on complete dehydration, produces a fluffy, voluminous, carbon-rich mass known as "precursor" powder. The chelating agent, EDTA, plays a critical role. It not only prevents the segregation or intermittent precipitation of metal ions from solution during evaporation but also acts as the fuel to provide the heat through combustion for the formation of the metal oxide phase. During thermal decomposition of precursor, nascent metal oxides forms, which are small atomic clusters with proper chemical homogeneity and these nascent metal oxides, finally produce Ni-Zn ferrite nanopowders. The heat provided by the carbonaceous mass of the precursor during thermal decomposition helps in lowering down of the external temperature required for the formation of the phase. Moreover, the evolution of various gases (such as water vapour, CO, CO_2, NO_x) during decomposition of the precursor helped it to disintegrate and dissipate the heat of decomposition. This inhibited the sintering of fine particles during the process to produce nanosized Ni-Zn ferrite [5, 7, 21].

DC resistivity measurements indicated that it was strongly correlated with the sintering condition and the composition and hence the microstructure of the samples. The resistivity of the nanopowders was found to be affected by moisture due to their high porosity and low green density (~2.5 g/cm^3). However, for the samples sintered at 1100^0C, the effect of moisture was less pronounced as sintering results in densification (sintered density~2.8-3.2 g/cm^3) and grain growth. For the samples sintered at an even higher temperature of 1200^0C, the effect of moisture was absent (sintered density ~3.4-4.2 g/cm^3) and the samples exhibited the typical NTCR behavior of ferrites, starting from room temperature.

4. Conclusions

Nanostructured, single phase Ni-Zn ferrite powders have been successfully synthesized by the EDTA precursor based method. The simplicity of this method makes it attractive as the method is based upon mixing and drying of aqueous solutions of starting materials followed by calcinations in air atmosphere. Wide range of compositions can easily be prepared by varying the amount of aqueous solution of the starting materials. The exquisiteness of the chemical method is that it produces single phase, Ni-Zn ferrite nanopowders (i) at comparatively low temperature (450^0C) (ii) by using inexpensive starting materials such as metal nitrates and distilled water as reaction medium and (iii) without using any elaborate experimental setup.

Microstructures and DC resisitivities of the series of $Ni_{1-x}Zn_xFe_2O_4$ ($0 \leq x \leq 1$) ferrites synthesized by EDTA precursor based method have been discussed in detail. The as-synthesized nanopowders (average particle size ~ 30 nm) were sintered in the temperature range of 1100-1300^0C. The microstructures of Ni-Zn ferrite nanopowders consisted of loosely bound agglomerates with large amount of open porosity and they exhibited high resistivity ~$10^7\Omega$cm. SEM micrographs of sintered samples of Ni-Zn ferrites revealed densified microstructures consisting of

large grains and nearly devoid of porosity. Resistivity of the sintered samples was ~10^6 Ωcm. Microstructures and resisitivities have been correlated and critically compared in order to emphasize the crucial differences between the unsintered nanopowders and sintered samples of Ni-Zn ferrites. Unlike other reported methods, Zn loss was not observed in SEM micrographs in our samples even at high sintering temperatures that ensure the quality and homogeneity of our as-synthesized samples. Room temperature magnetization measurement indicated a decrease in saturation magnetization with increase of zinc content in the samples.

Acknowledgements

N N Ghosh gratefully acknowledges support from Defense Research and Development Organization (Project number: ERIP/ER/0904500/M/01/1204), India. We also express our thanks to Dr. Rahul Mohan, National Center for Antarctica and Ocean Research, Goa, India, and Dr. Rosilda Selvin, Chemical and Materials Engineering Department, Lunghwa University of Science and Technology,Taoyuan County 333, Taiwan (ROC) for recording SEM and TEM micrographs of the samples, respectively.

References

[1] J. Smit, H.P. J. Wijn, Ferrites, Cleaver-Hume Press Ltd., London (1959).
[2] P. P Sarangi, B. Naik, S. R. Vadera, M. K. Patra, C. Prakash, N. N. Ghosh, Mater. Tech., Adv. Perform. Mater. (2009) DOI 10.1179/106678509X12519671504700
[3] C. Scherer, A. M. F. Neto, Braz. J. Phys. **35**, 718 (2005)
[4] P. Pant, S. Bhuvaneswari, N. N. Ghosh, Recent Patents Nanotechnol. **2**, 1 (2008)
[5] P. P. Sarangi, B. D. Naik, N. N. Ghosh, J. Am. Ceram. Soc. **91**, 4145 (2008**)**
[6] P. P. Sarangi, S. R Vadera, M. K. Patra, C. Prakash, N. N. Ghosh, J. Am. Ceram. Soc. **92**, 2425 (2009)
[7] P. P. Sarangi, B. D. Naik, N. N. Ghosh, Powder Technol. **192**, 245 (2009)
[8] P. Pant, B. D. Naik, N. N. Ghosh, Mater. Tech.: Adv. Perform. Mater., **24**, 213 (2009)
[9] P. P Sarangi, B. D. Naik, S. R. Vadera, M. K Patra, C Prakash, N. N. Ghosh, Mater. Tech.: Adv. Perform. Mater. **24**, 97 (2009)
[10] N. N. Ghosh, P. P. Sarangi, in Nanomaterials: Properties, Preparation and Processes, ed. By V. Cabral, R. Silva, Nova Publishers, New York (2010) (In press)
[11] N. N. Ghosh, P. P. Sarangi, in Combustion Synthesis: Novel Routes to Novel Materials, ed. By M.Lacner Bentham Science Publishers Ltd., Bussum (2010) (In Press)
[12] B. P. Rao, K. H. Rao, J. Mater. Sci. **32**, 6049 (1997).
[13] A. Verma, T.C. Goel, R. G. Mendiratta, R.G. Gupta, J. Magn. Magn. Mater.**192**, 271 (1999)
[14] R. V. Mangalaraja, S. Ananthakumar, P. Manohar, F. D. Gnanam, J. Magn. Magn. Mater. **253**, 56 (2002)
[15] T. J. Shinde, A. B. Gadari, P. M. Vasambekar, Mater. Chem. Phys. **111**, 87 (2008)
[16] A. D. Sheikh, V. L. Mathe, J. Mater. Sci. **43**, 2018 (2008)
[17] A. M. Kumar, M. C. Varma, C. L. Dube, K. H. Rao, S. C. Kashyap, J. Magn. Magn. Mater. **320**, 1995 (2008)
[18] A. Verma, R. Chatterjee, J. Magn. Magn. Mater. **306**, 313 (2006)
[19] C. Cantalini, M. Faccio, G.Ferri, M. Pelino, Sens. Actuators, B, **18-19,** 437 (1994)
[20] N. Rezlescu, E. Rezlescu, C. Doroftel, P. D. Popa, J. Phys: Conf. Ser. **15**, 296 (2005)
[21] P. Pramanik, A. Pathak, Bull. Mater. Sci. **17**, 967 (1994)
[22] A. S. Albuquerque, J. D. Ardisson, W. A. A. Macedo, J. Appl. Phys. **87**, 4352 (2000)
[23] A.Verma, T. C.Goel, R. G.Mendiratta, P. Kishan, J. Magn. Magn. Mater. **208**, 13 (2000)

*Corresponding author: naren70@yahoo.com